Development and Validation of a High Fidelity Finite Element Model of Monopolar Stimulation in the Implanted Guinea Pig Cochlea

Paul Wong, Shefin George, Phillip Tran, Andrian Sue, Paul Carter, and Qing Li*

***Abstract*—To better understand the key parameters affecting intracochlear electrode array performance, reliable electro-anatomical models are required. In this study, a high fidelity finite element model of the implanted guinea pig cochlea was generated from sTSLIM images and analyzed in COMSOL Multiphysics. The *in silico* model was then validated against independently obtained *in vivo* voltage tomography data. It was found that the simulation outputs were most sensitive to the resistivities of bone, perilymph, and nerve. Bone tissue in particular should be separated by morphology because different types of bone have different electrical properties. Despite having a strong impact on terminal voltages and current exit pathways, most boundary conditions, including a new alternative proposed to account for the unmodeled return path, only had a weak effect on predictions of neural excitation. These findings address a long-standing knowledge gap in the literature about appropriate boundary conditions, and the strong correlation between the new model and the *in vivo* data should help to promote wider acceptance of insights from computational models of the cochlea.**

***Index Terms*—Boundary conditions, cochlear implants, electrical stimulation, finite element analysis, image segmentation.**

I. Introduction

IN biomedical engineering, computational models are often less able to accurately predict outcomes than in other fields of engineering because the complex nature of biophysical interactions makes them more difficult to represent mathematically. Nevertheless, when used in conjunction with *in vivo* studies and bench-top testing, *in silico* studies have proven invaluable for obtaining a holistic understanding of medical devices since they enable experiments that would be impossible to perform using other methods [1]–[2].

Cochlear implant (CI) design is one area of research where *in silico* models are particularly useful. Despite advances in speech processing techniques [3], sentence recognition scores have plateaued for almost two decades, suggesting that there is a bottleneck at the electrode-tissue interface [4]. As such, the key to improving future performance is a greater spatial understanding of how current injection affects the auditory neurons [2]. *In vivo* methods are not ideal for this because the human inner ear is intricate and difficult to access surgically. Many studies have been performed on animals like the guinea pig, whose cochlea is easily exposed in the tympanic bulla [5], but still the invasive nature of experimental probing cannot reveal detailed current pathways. *In silico* investigations in the form of volume conduction models (VCMs) approach the problem from a different perspective and can overcome some of these challenges. Existing VCMs of both human and guinea pig cochleae [2], [6]–[16] have yielded many useful insights, but there is a reluctance to trust their findings in the research community. This is probably due to a range of factors, including the crude geometry of some existing models, unfamiliarity with computational methods, insufficient justification of assumptions, and the limited ability of models to predict psychophysical outcomes with consistent accuracy.

The primary goal of this paper is to introduce a new finite element (FE) model of the implanted guinea pig cochlea, and to compare its *in silico* predictions against similar *in vivo* voltage tomography data obtained independently at the Bionics Institute in Melbourne, Australia. If a good correlation between the *in silico* and *in vivo* results is found, confidence in the new FE model will be established, and some of the concerns surrounding the use of VCMs may be alleviated.

The correlation is expected to be strong because the new model includes several improvements over previous models. Existing VCMs typically use histological sections traced and swept along a spiral path, or a simplified computer-aided design (CAD) geometry. This model was reconstructed from a stack of scanning thin-sheet laser imaging microscopy (sTSLIM) images [17], so the geometry is considerably more realistic: the hook region is accurately represented and includes the round window membrane and the stapes; the scala tympani and scala vestibuli are truly continuous at the helicotrema; the major blood vessels and cerebrospinal fluid (CSF) in the modiolus were incorporated—unique for VCMs of the cochlea. Furthermore, bone was not treated as a homogeneous material, but instead separated into the modiolar bone, the otic capsule, and the temporal bone. These have markedly different microstructures and hence different

Submitted for review on 18 December 2014. Revised on 19 May 2015 and 2 August 2015. This work was supported in part by the Australian Research Council through a Linkage Scheme (LP0776938).

P. Wong (email: paul.wong@sydney.edu.au), P. Tran, A. Sue, and *Q. Li (corresponding author, email: qing.li@sydney.edu.au) are with the School of Aerospace, Mechanical and Mechatronic Engineering, The University of Sydney, Camperdown, NSW 2006 Australia.

S. George is with the Bionics Institute, Melbourne, VIC 3002 Australia (email: sgeorge@bionicsinstitute.org).

P. Carter is with Implants Development at Cochlear Limited, Sydney, NSW 2109 Australia (email: pcarter@cochlear.com).

TABLE I
SEGMENTED TISSUE TYPES AND BASE RESISTIVITY VALUES

Material *(included structures)*	Base Resistivity (Ω.m)	Source
Bone		
Modiolar bone	11.7	Suesserman [20]
Otic capsule	6.41	Suesserman [20]
Temporal bone	13.73[a]	Suesserman [20]
Perilymph *(scala tympani, scala vestibuli)*	0.7	Finley [5]
Endolymph *(scala media, vestibule)*	0.6	Finley [5]
Nerve *(cochlear nerve trunk, spiral ganglion, peripheral processes)*	3	Finley [5]
Cerebrospinal fluid (CSF)	0.56	Gabriel [21]
Blood *(spiral modiolar artery, vein of the scala tympani)*	1.5	Mohapatra [22]
Spiral ligament	0.6	Frijns [7]
Stria vascularis	188.685	Frijns [7]
Organ of Corti	83.333	Frijns [7]
Basilar membrane	80	Finley [5]
Reissner's membrane	10,204	Finley [5]
Round window membrane	1,000[b]	—
Silicone	1×10^{7}	
Platinum	1.06×10^{-7}	

[a]Based on Suesserman's measurement for the guinea pig skull.
[b]No data available; estimate based on values of other membranous tissues.

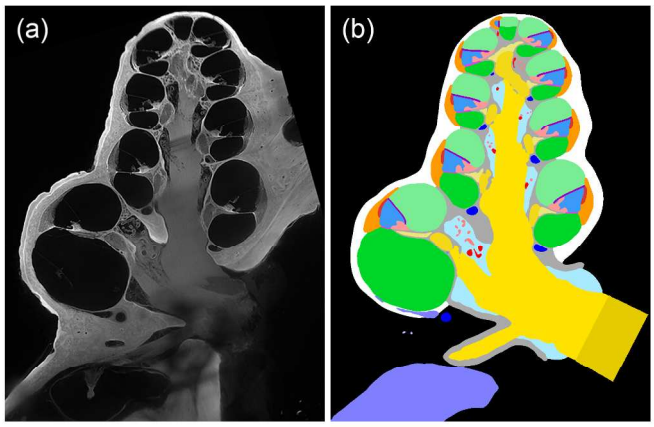

Fig. 1. A mid-modiolar slice from (a) the original sTSLIM image stack, and (b) the corresponding segmentation.

electrical resistivities, so they should be treated as separate material domains [4], [15], [18].

The secondary goal of this paper is to evaluate the validity of long-held assumptions on material properties and boundary conditions. These two factors are important in determining the *in silico* results for any particular geometry.

Like previous studies, this model assumes that the cochlear tissues are purely resistive, based on the evidence provided by Spelman [19]. Resistivity values from the literature (Table 1) are used as base values. There are no measurements in the literature for the round window membrane, which is being incorporated into a VCM for the first time. To determine the impact of any measurement uncertainties, as well as natural variations in properties between individuals, the sensitivity of the model to each tissue resistivity value was evaluated.

Boundary conditions are modeling constraints necessary for solving the field problem [23] and should ideally replicate the physics at the boundary of the modeled domain accurately. This is problematic for VCMs of the cochlea simulating monopolar (MP) stimulation because the return electrode lies outside the physical domain of the model. Existing models deal with this issue by assuming that the end of the auditory nerve is grounded [2], [12], that the ground is infinitely far away [8], or that boundary box surfaces are grounded [10], [14]—none of these perfectly match the *in vivo* situation. Alternatively, they avoid the MP situation altogether and focus on pseudo-monopolar or bipolar stimulation [5]–[7], [9], [11]. Although the simulation results in these cases are indicative, they are less clinically relevant given the widespread use of MP stimulation in CI recipients. To clarify how the boundary condition assumption affects simulation results, several different cases, reflecting the range of existing choices as well as more realistic alternatives, are compared to provide some guidance for future modeling efforts.

II. METHOD: IN SILICO MODELING

A modular workflow based on that established by Tran *et al.* [16] was adopted in order to overcome the segmentation and meshing challenges typically encountered in electro-anatomical modeling [24]. The best features of several programs were selectively combined to create a more accurate model than would otherwise have been possible.

A. Imaging and Reconstruction

A high resolution (4.625×4.625×5 μm voxel size) sTSLIM image stack of the guinea pig cochlea was obtained from The University of Minnesota, USA [see Fig. 1(a)]. This technique combines the high resolution and clarity of optical microscopy with the non-destructive nature of computed tomography (CT) and magnetic resonance imaging (MRI), making it ideal for capturing fine anatomical details [17], [25]. The cochlea was explanted from a healthy guinea pig, with no visible scar tissue and only minor neuronal degeneration at the basal end. Both soft and hard tissues were identifiable, and the images were predominantly free of absorption artifacts.

Fourteen different tissue types were then identified and segmented [see Table 1 and Fig. 1(b)] using a semi-manual process in Amira v5.4.2 (Visualization Sciences Group, Burlington MA, USA). For each tissue, a region in one image was selected with the aid of luminance thresholds. The selection was then smoothed, and the process repeated on the adjacent slice. If there was minimal variation in shape between successive slices, the next selection would be made several slices away and the volume in between was selected via interpolation. This preserved the organic appearance of the tissues while reducing the amount of data to be processed. Perilymph, endolymph, nerve, and blood were subcategorized by anatomical structure to aid visualization. The thin membranes between the scala vestibuli and the vestibule were excluded in this reconstruction, as per other models. Finally, some additional smoothing was applied, and any remaining voxel fragments were allocated to adjacent masks to ensure continuity throughout the volume in preparation for mesh generation.

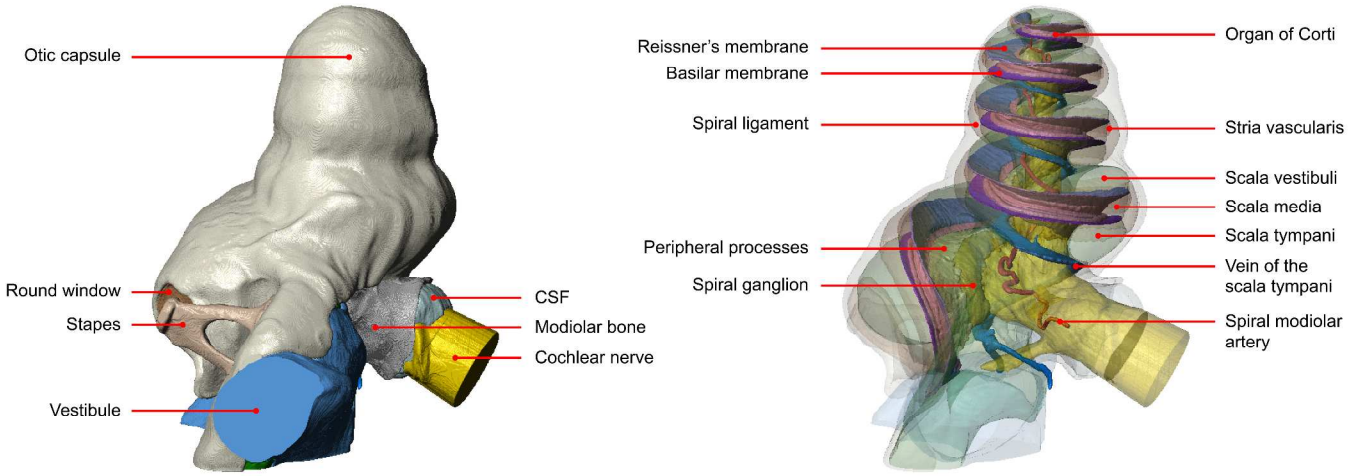

Fig. 2. Reconstruction of the healthy guinea pig cochlea. The complex internal structures are clearly seen on the right. Note that the cerebrospinal fluid (CSF) and modiolar bone encase the nerve tissue as per Fig. 1(b), but these are shown with transparency here to reveal the major blood vessels.

The segmented domains were exported into ScanIP v4.3 (Simpleware Limited, Exeter, UK), and a surface model was generated from the binarized masks in a stereolithography (STL) format. The pre-smoothing and part change options were enabled to avoid jagged surfaces, and decimation was disabled to ensure conformity between adjacent components. The resulting reconstruction is shown in Fig. 2.

B. *Mesh Generation*

The STL files were imported into ICEM CFD v15.0 (ANSYS Incorporated, Canonsburg PA, USA) for volume meshing. Since orthogonal surfaces artificially draw current toward the center of each face [26], the tissues were embedded in a sphere to facilitate the application of more realistic boundary conditions. Unlike the human cochlea, which is encased within the temporal bone, the guinea pig cochlea protrudes into the tympanic bulla [5], so injected current must flow medially towards the temporal bone. The surrounding sphere was therefore angled such that one hemisphere extended into the tympanic bulla and the other into the surrounding temporal bone [hereafter referred to as the "temporal bone surface"; see inset, Fig. 9(c)], matching the bone boundary in the scans.

A CAD model resembling the Cochlear Limited Hybrid-L8 (HL8) electrode array was inserted through the round window and into the scala tympani in a mid-scala position. Electrodes were numbered from E1 at the basal end to E8 at the apical end. Insertion depth was just over 6 mm, corresponding to an insertion angle of about 380 degrees at E8. A "build topology" operation was performed to ensure that the mesh respected the smooth curves of the array model.

Element sizes for each component were established to balance node count against geometrical accuracy. A volume mesh was then generated using ICEM CFD's top-down Octree algorithm. Finally, any small element islands resulting from the process were assigned to an adjacent domain.

C. *Finite Element Analysis*

A base case was first defined as a reference for comparison of the *in silico* results. All tissue domains were configured with isotropic resistivities as in Table 1. A 1 mA constant current source was placed at the inner surface of the stimulating electrode, identical to that used for the *in vivo* measurements. The external surface of the round window membrane was insulated to prohibit current flow from the scala tympani into the non-conductive middle ear air space, as expected *in vivo*. Lastly, the temporal bone surface was grounded to represent the expected MP current sink.

A convergence test was then performed to ensure sufficient discretization. Five meshes were generated using different element size limits and imported into COMSOL Multiphysics v4.3 (COMSOL AB, Stockholm, Sweden) in the NASTRAN format. Both the PARDISO (direct) and Conjugate Gradient (iterative) solvers were tested, with no observed difference in numerical results. PARDISO just exceeded the computer's RAM capacity when solving quadratically discretized meshes, so the Conjugate Gradient solver was used to prevent writing to disk. Simulations were run on a Windows 7 workstation with an Intel Core i7 3930K CPU and 64 GB of RAM.

Using the converged mesh, both material properties and boundary conditions were altered *ceteris paribus* from the base case. For the sensitivity analysis on material properties, individual tissue resistivities were set to either double or half of the base value (à la Finley [27] and Rattay [10]), or the highest or lowest values from literature, whichever deviated more from the base value. Since there was no data for the round window membrane, its resistivity was assumed to be 1000 Ω.m based on the geometric average of Reissner's membrane and the basilar membrane (see Table 1), and an order of magnitude variation was tested to account for the additional uncertainty.

For the boundary condition tests, the base case was rerun with each of the following boundary conditions (shown as insets in Fig. 9):

1) Ground the auditory nerve trunk only;
2) Ground the caudal aspect of the temporal bone surface;
3) Ground the entire temporal bone surface;
4) Apply a voltage offset on the temporal bone surface;
5) Ground the entire outer surface of the surrounding sphere;
6) Ground at an infinitely large surrounding sphere.

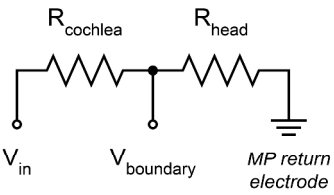

Fig. 3. The modeled domain only includes the resistance inside the cochlea. For MP stimulation, injected current must also overcome the resistance of the head to reach ground, so the voltage at the boundary should be non-zero.

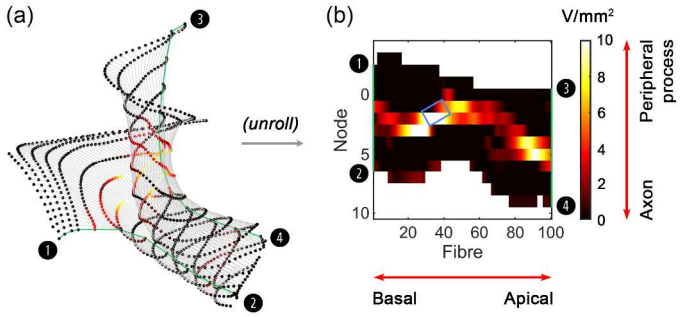

Fig. 4. (a) 3D representation of the neural sheet, with fibers 1 and 100 traced in green; (b) the corresponding 2D plot. The coordinate system follows that of Kalkman *et al.*, except here Rosenthal's canal is always located at node 0. The location of the active electrode is marked by the blue box.

Boundary conditions 2–5 were applied on a surrounding sphere of radius 5 mm because this size was found to be sufficiently large for replicating far-field effects [26]. For grounding at infinity, a second shell of radius 8 mm was added and configured as an infinite element domain in COMSOL, with resistivity set to that of the guinea pig skull [20].

The voltage offset boundary condition is a novel proposal. In a real CI recipient, the stimulating current must pass through the cochlear tissues as well as the rest of the head in order to reach the return electrode under MP stimulation (see Fig. 3). If the resistance of the head is not accounted for in the model, the total resistance will be underestimated. The circuit can is also a voltage divider, so given the non-zero resistance of the head, the electric potential at the model boundary should also be non-zero (i.e. not grounded). The offset value for these simulations was determined as the average difference in terminal voltages between grounding at the temporal bone surface and the mean *in vivo* profile.

The primary model output was the average voltage at each electrode, because this could be directly compared with the *in vivo* results. The magnitude and direction of current flow were depicted using streamline plots of current density seeded on a regular quadratic grid over the surface of the active electrode. Neuron trajectories covering the first 570 degrees of the cochlea were modeled in MATLAB (The Mathworks Inc., Natick MA, USA) by connecting key points from the tips of the peripheral processes, through the cross-sectional center of the spiral ganglion, and down along the cochlear nerve trunk [see Fig. 4(a)], similar to Kalkman *et al.* [28]. For each neuron, nodes of Ranvier were placed at fixed intervals from the point in Rosenthal's canal. Spacing resembled that used in the GSEF neural model [7]: 175 µm along the peripheral process and 300 µm along the axon. The activating function (AF), i.e. the discrete second derivative of electric potential with respect to distance along the fiber [29], was computed for each set of adjacent nodal triads along 100 equally spaced fibers. It signifies the degree to which the underlying electrophysiological requirements for neural firing are met.

III. Method: In Vivo Measurements

Voltage tomography measurements were collected from eight (N=8) adult pigmented guinea pigs (500–800 g) for comparison with the *in silico* results. All procedures were approved by the Royal Victorian Eye and Ear Hospital Animal Research and Ethics Committee and were in accordance with the Australian Code of Practice for the Care and Use of Animals for Scientific Purposes. All procedures were performed in an electrically isolated Faraday room.

The animals were anaesthetized using isoflurane (1.5–2%) and oxygen (1 L/min). Respiration rate (normal levels: 15–25 breaths/min) and end-tidal CO_2 levels (normal levels: 1–3%) were monitored over the duration of the experiment (2–3 hours). Core body temperature was maintained at 37.0 ± 1°C. A post-auricular incision was made and the left cochlea was surgically exposed. Each animal was implanted with an HL8 array, containing eight intracochlear platinum half-band electrodes on a silicone carrier. The electrode array was inserted approximately 6 mm through the round window into the scala tympani, typically placing 7–8 electrodes within the scala. A platinum ball electrode placed in the neck muscles served as the MP return and reference electrode.

For each intracochlear electrode, a monopolar cathodic-first biphasic pulse (25 µs per phase and 8 µs inter-phase gap) was delivered with an amplitude of 1 mA. The voltage at each of the non-stimulating electrodes was measured with respect to the reference electrode at the end of the cathodic phase. The voltage at the stimulating electrode was estimated as the maximum among the values extrapolated from all available adjacent pairs, as adapted from van den Honert and Kelsall [30], to ensure that the sharpness of the current spread function was not underestimated.

IV. Results

A. In vivo data

The raw measurements for all eight guinea pigs during stimulation at E4 are shown in Fig. 4. (Only results at E4 are presented for brevity.) Differences between guinea pigs were observed, presumably due to the unique geometry of each cochlea and its surrounding tissues, variations in the surgical insertion of the implants and the resistivity of the tissues, and other subject-specific factors. Most of the profiles clustered around the average, so a mean profile was calculated to serve as a benchmark for comparison with the *in silico* results. The minimum to maximum voltage range over all specimens was also found and is shaded in Fig. 5.

The apical electrode (E8) was excluded from the comparisons because measurements from that electrode could not be obtained in four of the eight guinea pigs. This was likely due to the electrode tip folding over during insertion.

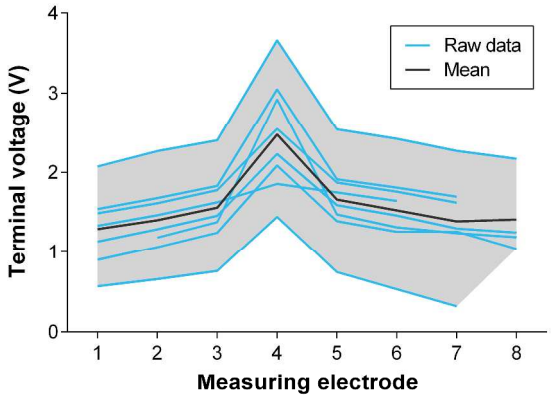

Fig. 5. *In vivo* voltage measurements (N=8) along the array during stimulation at E4. Shortened traces are due to tip fold-over or incomplete insertion. The shaded area represents the spread of *in vivo* results.

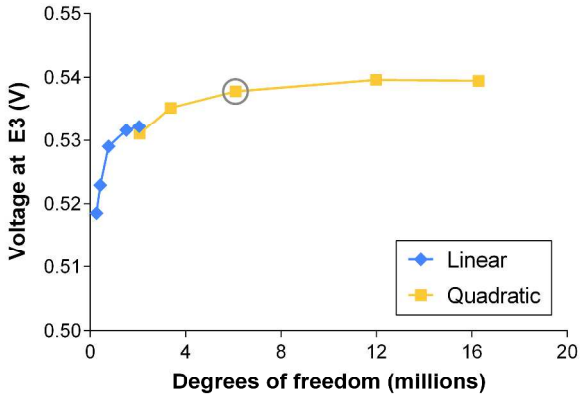

Fig. 6. Mesh convergence results for voltage at E3 during stimulation at E4. The selected mesh (circled) exhibits only 0.3% difference relative to the densest quadratic mesh (far right), and is considered converged.

B. *Mesh Convergence*

Each mesh was solved using both linear and quadratic elements. The coarsest linear mesh had 262,620 degrees of freedom (DOFs) and the finest quadratic mesh had 16,278,789 DOFs, taking 12 seconds and 2 hours respectively to compute.

Fig. 6 indicates that the mesh with 6,092,537 DOFs is well converged, with only 0.3% difference relative to the densest quadratic mesh that was tested. Solution time was about 30 minutes, striking a good balance between accuracy and computational cost. All of the linearly discretized meshes exhibited greater than 5% difference, suggesting that linear shape functions were insufficient for capturing the electric field behavior in this model (cf. Frijns [7]).

C. *Sensitivity of Terminal Voltage Predictions*

Table 2 shows the percentage impact of tissue properties on terminal voltage predictions. These values were calculated relative to the base case and classified as either negligible (less than 0.5% difference), weak (0.5–5%), or strong (more than 5%). For this model, the resistivities of most tissues had either a negligible or weak effect on terminal voltages. The exceptions were bone, perilymph, and nerve. Temporal bone resistivity was the most sensitive, with differences of up to 90.8% relative to the base case. At extreme literature values for otic capsule resistivity [31], [32], up to 59% difference was observed. Treating bone with a homogeneous resistivity of 6.41 Ω.m underestimated terminal voltages relative to the base case [see Fig. 7(a)]. Perilymph had a particularly strong effect at the stimulating electrode and was notably the only tissue to change the shape of the profile. Nerve resistivity had up to 5.79% impact on terminal voltages.

Fig. 7(b) compares the *in silico* and *in vivo* terminal voltages for each of the tested boundary conditions. Again, the shape of the profile did not change significantly. A wide spread of voltage magnitudes was observed, however. Grounding at infinity or at the nerve trunk overestimated voltages along the array, relative to the observed *in vivo* mean. In contrast, grounding the surrounding sphere or part thereof led to substantial underestimates, with smaller grounding areas corresponding to higher terminal voltages. Some of these fell outside the range of observed *in vivo* measurements. Offset values required to match the *in vivo* average were found to vary with the location of current injection, as shown in Fig. 8. For stimulation at E4, a 0.905 V offset on the temporal bone surface yielded a close match to the *in vivo* measurements.

TABLE II
SENSITIVITY OF TERMINAL VOLTAGES TO TISSUE RESISTIVITIES

Tissue	Deviation from Base Case (%)	
	Mean	Max
Bone (homogeneous, ρ = 6.41 Ω.m)	43.2	51.0
Modiolar bone[a]	1.76	3.60
Otic capsule[b] (ρ = 1.5–350 Ω.m)	50.7	59.0
Temporal bone[a]	73.9	90.8
Perilymph[a]	10.3	47.2
Endolymph[a]	0.51	0.65
Nerve[b] (ρ = 1–7.14 Ω.m)	3.18	5.79
CSF[a]	0.83	1.06
Blood[b] (ρ = 0.61–5.56 Ω.m)	0.18	0.61
Spiral ligament[b] (ρ_U = 2.5 Ω.m)	2.03	2.99
Stria vascularis[b] (ρ_L = 3 Ω.m)	0.28	0.42
Organ of Corti[a]	0.08	0.14
Basilar membrane[a]	0.03	0.06
Reissner's membrane[a]	0.02	0.04
Round window membrane[c]	0.02	0.05

[a]Resistivity changed from base value by a factor of two.
[b]Upper (ρ_U) and lower (ρ_L) resistivity limits based on extreme values from literature, as indicated.
[c]Resistivity changed from base value by a factor of ten.

D. *Effect on Current Pathways*

Streamline plots revealed that current spread in the near-field was relatively insensitive to both tissue properties and boundary conditions, leading to similar gradients of voltage falloff as shown in Fig 7. Beyond the scala tympani however, current flow patterns were noticeably different. Fig. 9 shows that current paths were strongly dependent on the prescribed boundary condition. Grounding the nerve [Fig. 9(a)] was the most distinct, with streamlines reconverging at the grounded nerve surface and an obvious edge effect around its periphery. Grounding the entire surrounding sphere [Fig. 9(d)] resulted in omnidirectional current spread beyond the cochlea, as did grounding at infinity [Fig 9(e)]. Restricting the grounding surface to a quadrant [Fig. 9(b)] or hemisphere [Fig 9(c)] imposed a sense of directionality on the exit pathway. Lastly, applying a voltage offset on the temporal bone surface [Fig. 9(c)] produced virtually identical streamlines as grounding it.

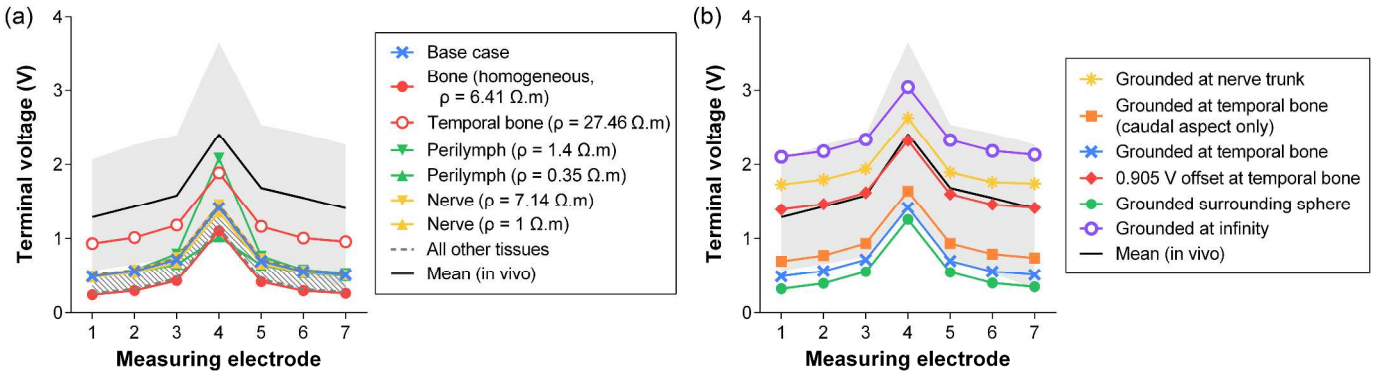

Fig. 7. Sensitivity of terminal voltages to (a) selected resistivity values, and (b) boundary conditions. Base case values are marked with blue crosses. The light grey areas represent the range of *in vivo* voltage measurements from Fig. 4. (a) Most tissues have little impact on the *in silico* predictions, and almost all data points fall outside the *in vivo* range. (b) Boundary conditions have virtually no effect on the shape of the profile, but strongly affect the voltage magnitudes.

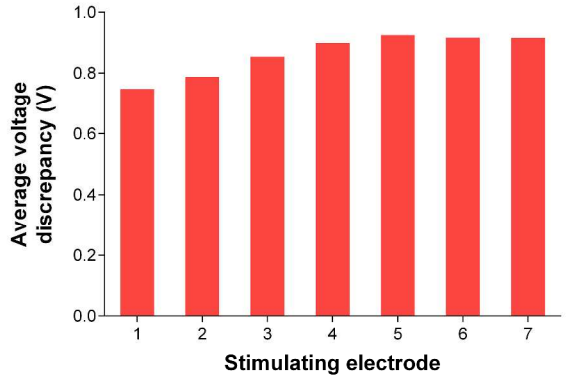

Fig. 8. The voltage offset required to match the mean in vivo results changes with the location of current injection. Offset values are lower for basal electrodes, and level off between E4 and E7.

E. Estimated Impact on Neural Excitation

Differences in current flow pathways in turn affected predictions of neural excitation as measured by the AF. The main regions of excitation were largely similar for any particular stimulating electrode, but localized differences along the neural sheet were also observed.

In this model, higher bone resistivity drove more current into the nerve tissue and increased the likelihood of firing [Fig. 10(a)–(c)] relative to the base case [Fig. 4(b)]. Likewise, higher resistivities for perilymph, nerve, or the spiral ligament altered the current distribution, leading to localized differences around the main area of excitation as well as increased axonal activity at fibers that originated one turn away [Fig. 10(d)–(f)]. Regarding boundary conditions, grounding the nerve trunk [Fig. 11(a)] resulted in significantly more widespread depolarization than in the other cases (+67.5% RMS, the largest discrepancy of all the test cases). The effects were especially pronounced near the end of the axon where the ground was imposed. AF values for the grounded temporal bone surface and the corresponding offset case were virtually identical, which was expected given their similar current pathways. A slightly larger discrepancy was observed between the sphere grounding and infinite grounding conditions [Fig. 11(c)–(d)]. However, boundary conditions 2–6 all produced AF patterns that were within about 5% of each other, suggesting that the model was not highly sensitive to this assumption.

V. Discussion

A. Modeling Workflow

The methodology used in this study allowed for a high fidelity reconstruction of the cochlea with an unprecedented amount of anatomical detail, but it also suffered from a few drawbacks stemming from the large size of the data set. Firstly, the time required to process the image stack was in the order of months due to the large number of tissues and the need for some sophisticated manual segmentation. Secondly, the segmentation process required comprehensive knowledge of the anatomy in the region of interest, and consultations with anatomical experts were needed to minimize the risk of incorrect reconstruction. Algorithmic segmentation could be employed in the future to reduce the time requirements and inconsistencies due to human error, but to the extent of the authors' knowledge, existing techniques are not well suited to datasets with many tissues and are usually optimized for CT or MRI image stacks. Thirdly, although the Octree algorithm was robust enough to handle the complexity of the surfaces, it always resulted in the production of some small element islands. While smoothing the segmentation eliminated some of these islands, the requirement for manual intervention limits the potential for a fully automated process.

Overall, the capabilities of this workflow far outweighed its limitations. It can be expected to translate well to other datasets and other organs, regardless of imaging modality.

B. Material Properties

There is some concern that the base resistivity values for cochlear-specific tissues may not be appropriate because the scaling and disregard of spatial effects necessary to derive them from bulk resistances compromises their accuracy [2], [4], [7]. Most values can also be traced back to a single source [33], so there is doubt over the reliability of the measurements.

According to the simulation results, the model is not very sensitive to most tissue resistivities. The spread of terminal voltage predictions in Fig. 7(a) is smaller than the standard deviation of the *in vivo* measurements, suggesting that any uncertainties are within inter-subject variability limits. The continued use of these values in the literature also suggests that they represent the electric behavior reasonably well.

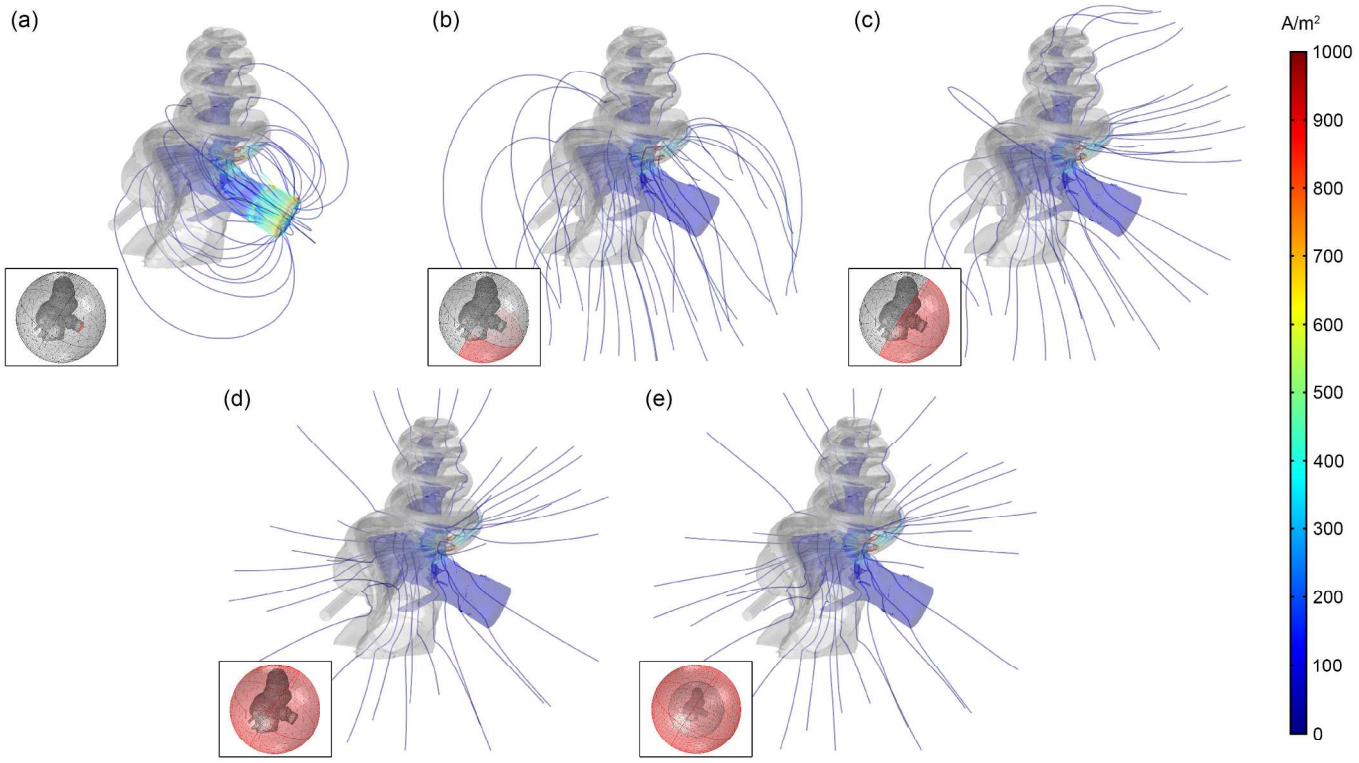

Fig. 9. Streamline plots showing the current paths during stimulation at E4 for (a) grounding the nerve trunk, (b) grounding the caudal aspect of the temporal bone surface, (c) grounding or applying a 0.905 V offset on the temporal bone surface, (d) grounding the entire surrounding sphere, and (e) grounding at infinity. Insets show the corresponding surfaces highlighted in red. The outermost domain in (e) is configured as an infinite element domain. Scale indicates current density in the nerve tissue.

For the tissues to which the model was sensitive, some (namely CSF, endolymph, and perilymph) have resistivities that are known accurately [7], [21] and can therefore be used with confidence. The FE model in this study was based on a healthy, unimplanted guinea pig cochlea, and the validation data was obtained from acute experiments, so the base value of perilymph resistivity was suitable. In chronic implants however, the perilymph around the electrode array is displaced by a layer of fibrous encapsulation tissue [34]. Given the sensitivity of the model to perilymph resistivity, this would have a bearing on predictions of stimulation thresholds [35].

Terminal voltages were most sensitive to the bone domains because injected current must pass through them to reach ground. As such, these values were particularly crucial. The Suesserman resistivity measurements [20] used in this study are specific to the guinea pig and, given the care with which they were taken, should be quite accurate. However, it is curious that the lateral wall was reported as being less resistive than the modiolar wall because higher density bone is more resistive [32] and the otic capsule is the densest bone in the body [36]. The use of the skull value for the temporal bone and infinite domains may also be an underestimate since the temporal bone is relatively dense. Conversely, the current path through the head is likely to follow lower resistance pathways, such as through the CSF [16]. Determining the true effect on the return pathway would require a whole head model.

The resistivity of the spiral ligament should also be verified. At 0.6 Ω.m, it is relatively low, reflecting the suspicion that perilymph can diffuse freely through it and that it is involved in ion transport [37]. However, considering the known presence of various cell types and extracellular matrix material in the tissue, and that perilymph itself has a resistivity of 0.7 Ω.m, this may be inaccurate. The only other estimate in the literature is 2.5 Ω.m [2]. At this higher resistivity, the scala media became more insulated, leading to differences in terminal voltages, current pathways, and AF. It may be worth investigating whether the scala media should be modeled as being insulated on all sides to represent the tight junctions between the surrounding epithelial cells that prevent ionic current flow *in vivo* [37].

The ideal resolution to these uncertainties over material properties would be to re-measure the resistivities of all the cochlear tissues using an accurate and up-to-date technique [38]. At the least, this would provide an alternative data point for comparison with the values derived from lumped-element models; at best, these values would form a new gold standard as inputs for future electroanatomical studies of the cochlea.

C. *Boundary Conditions*

Three criteria were considered for evaluating the boundary conditions: closeness of match to the *in vivo* terminal voltages [Fig. 7(b)], the current paths exiting the cochlea (Fig. 9), and the impact on AF values (Fig. 10 and 11).

Grounding the nerve trunk seemed to make sense based on early evidence that the nerve trunk is the dominant exit pathway [39]. Using this boundary condition, simulated voltages were relatively high because current was forced to flow through a small return area. However, the otic capsule is

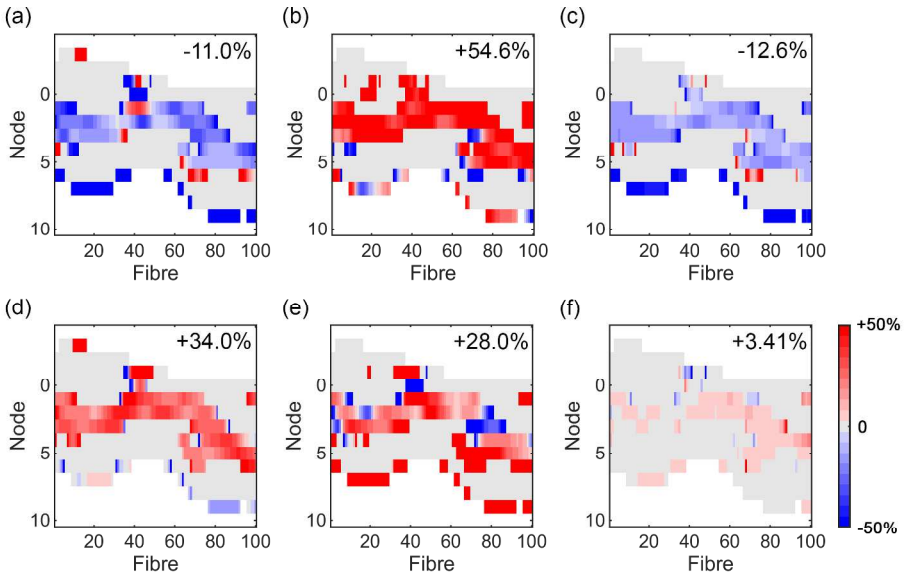

Fig. 10. Percentage difference in activating function relative to the base case [Fig. 4(b)]. Consistently hyperpolarized regions were considered unchanged. Selected tissue resistivity cases are shown: (a) homogenous bone (ρ=6.41 Ω.m), (b) otic capsule (ρ=350 Ω.m), (c) temporal bone (ρ=6.865 Ω.m), (d) perilymph (ρ=1.4 Ω.m), (e) nerve (ρ=7.14 Ω.m), and (f) spiral ligament (ρ=2.5 Ω.m). RMS differences are shown in the top-right corner.

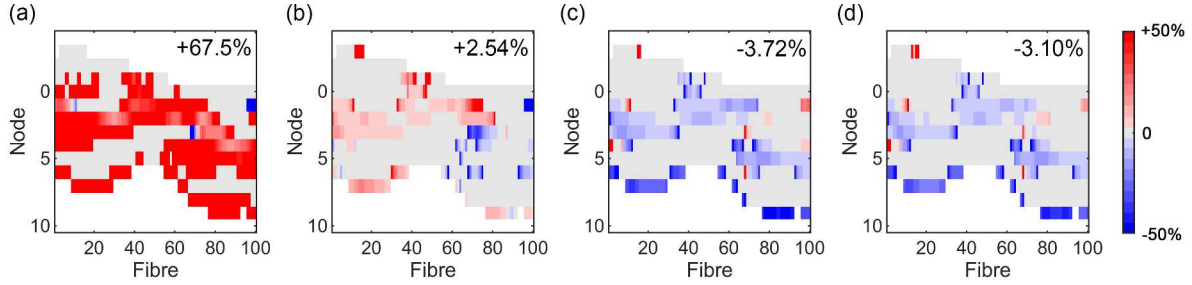

Fig. 11. AF deltas for selected boundary conditions, with grounding at (a) the cochlear nerve, (b) the caudal aspect of the temporal bone surface, (c) the surrounding sphere, and (d) at infinity.

not a perfect insulator and both the stimulating and return electrodes are small relative to the head, so injected current spreads out as it flows through the cochlear tissues and is not expected to re-converge within the domain [16], [40] as observed in Fig. 9(a). Because of this, the AF plot [Fig. 11(a)] predicted substantially more widespread depolarization than the other boundary conditions. Combined with the relative proximity of this isosurface to the regions of interest within the domain, it appears that this boundary condition violates Saint-Venant's Principle of far field equivalence by not faithfully reproducing true MP loading patterns. The evidence suggests that grounding the end of the modeled nerve trunk is inappropriate, at least in the case of the guinea pig cochlea.

Simply grounding an outer surface to represent the current sink is also insufficient. It ignores the presence of the return path through the head and thus underestimates intrascalar voltages [Fig. 7(b)]. Including the return path as an infinite domain is plausible, but tends to overestimate voltages. Of course, this depends on the resistivity of the infinite domain, and a value could be applied that forces a match with the *in vivo* data, but that would alter the ratio of resistivities between the temporal bone and other cochlear tissues, which could result in unintended effects on the current paths within the cochlea [4], [15] and the AF [e.g. Fig. 10(b)]. This is not ideal because resistivities are not a variable and can be measured. The value used for the infinite element domain in this study appears to be higher than the effective resistivity of the mean guinea pig head. In any case, purely grounded boundary conditions cannot be easily matched to *in vivo* data, which may be important in future subject-specific modeling efforts.

Given that none of the above boundary conditions presented a close match to the *in vivo* data, the voltage offset was proposed and tested. This alternative explanation for the voltage drop along the unmodeled return path through the head did not seem to influence the current pathways or AF, presumably because it is canceled out in the calculation. Its value could therefore be set arbitrarily to model different cases, as required for subject-specific models. The principle could also be applied to cochlear models from other species.

The offset would ideally be applied to a grounding surface that replicates the *in vivo* current paths. In these simulations, grounding the temporal bone surface was considered to be the most realistic because the protrusion of the guinea pig cochlea into the tympanic bulla, the low voltages exhibited during CI stimulation, and the extremely high impedance of air together suggested that injected current would flow away from the bulla [Fig 9(c)]. However, there is no way to be sure without implementing a complete guinea pig head model.

Ultimately, grounding surfaces need to be sufficiently large and far from the stimulating electrode in models of MP stimulation to prevent adverse impacts on the computed AF.

D. Study Limitations

The trajectory of the electrode array within the scala tympani was unlikely to be a perfect match despite taking care to accurately replicate the insertion at the round window. HL8 arrays tend towards a more lateral position, but the exact *in vivo* positions of each electrode were not confirmed in this study. Each insertion was also slightly different, and the data for more apical stimulation suggest that the modeled insertion was slightly deeper than the *in vivo* average. This adds a little uncertainty to the *in silico* predictions, but the close fit inspires confidence in the model nonetheless.

Another concern was that the *in vivo* measurements were taken at the end of the stimulating phase. It is known that the voltage profile changes over the duration of the pulse, and there is some speculation that time-dependent effects may play a role despite Spelman's observations [19]. Until this hypothesis is tested, the purely resistive formulation of this model should only be taken as a first approximation.

Lastly, the sample size for the *in vivo* measurements was relatively small. Ideally, more measurements would be added to the comparison to increase the statistical power, but this must be balanced against the financial, time, and ethical costs of obtaining these additional data points. It is hoped that if *in silico* models such as the one presented here become sufficiently accurate and trustworthy, the reliance on animal testing may be reduced in the long term.

VI. Conclusion

The workflow used in this study successfully overcame the difficulties seen in other *in silico* modeling methodologies to enable the creation of a high fidelity FE model of the guinea pig cochlea. Intrascalar voltages predicted by the model were more sensitive to the choice of boundary condition than to the assigned tissue resistivity values. However, the AF along the neural sheet was more sensitive to certain material properties. Grounding the nerve trunk appeared to be inappropriate for the guinea pig model; conversely, the proposed voltage offset boundary condition was able to characterize multiple facets of the *in vivo* situation realistically. In addition, the offset provides a feasible method for accommodating subject-specific differences, and may therefore be considered for use in future models of monopolar CI stimulation. Overall, the strong correlation between the *in silico* results and the average *in vivo* measurements indicated that the model can be used to represent an average implanted guinea pig cochlea.

Acknowledgment

The authors would like to thank Peter Santi at the University of Minnesota for obtaining the sTSLIM scans, Jonathon Kirk at Cochlear Americas for sharing them, Nick Pawsey and Joe Giorgio at Cochlear Limited for providing access to Amira and generating CAD models of the electrode array.

References

[1] U.S. Food and Drug Administration. (2012, May). Computational Modeling in Medical Devices. Presented at ASME V&V Symposium. [Online]. Available: https://cstools.asme.org/CSConnect/FileUpload.cfm?View=yes&ID=36699.

[2] G. Girzon, "Investigation of current flow in the inner ear during electrical stimulation of intracochlear electrodes," M.S. thesis, Dept. Elect. Eng. & Comp. Sci., MIT, Cambridge, MA, 1987.

[3] F. G. Zeng *et al.*, "Cochlear implants: System design, integration, and evaluation," *Rev. Biomed. Eng.*, vol. 1, pp. 115–142, 2008, DOI:10.1109/RBME.2008.2008250.

[4] A. G. Micco and C. P. Richter, "Tissue resistivities determine the current flow in the cochlea," *Curr. Opin. Otolaryngol. Head Neck Surg.*, vol. 14, no. 5, pp. 352–355, 2006.

[5] G. Cooper and A. L. Schiller, *Anatomy of the guinea pig*, Cambridge, MA: Harvard University Press, 1975.

[6] C. C. Finley *et al.*, "Models of neural responsiveness to electrical stimulation," in *Cochlear Implants*, New York: Springer, 1990, pp. 55-96.

[7] J. H. M. Frijns *et al.*, "Potential distributions and neural excitation patterns in a rotationally symmetric model of the electrically stimulated cochlea," *Hear. Res.*, vol. 87, no. 1, pp. 170–186, 1995.

[8] J. H. M. Frijns *et al.*, "Integrated use of volume conduction and neural models to simulate the response to cochlear implants," *Simulat. Pract. Theory*, vol. 8, no. 1-2, pp. 75–97, 2000.

[9] T. Hanekom, "Three-dimensional spiraling finite element model of the electrically stimulated cochlea," *Ear Hear.*, vol. 22, no. 4, pp. 300-315, 2001.

[10] F. Rattay *et al.*, "A model of the electrically excited human cochlear neuron. II. Influence of the three-dimensional cochlear structure on neural excitability," *Hear. Res.*, vol 153, pp. 64-79, 2001.

[11] C. T. M. Choi *et al.*, "Optimization of cochlear implant electrode array using genetic algorithms and computational neuroscience models," *IEEE Trans. Magn.*, vol. 40, no. 2, pp. 639–642, 2004.

[12] D. M. Whiten, "Electro-anatomical models of the cochlear implant," Ph.D. dissertation, Div. of Health Sci. & Tech., MIT, Cambridge, MA, 2007.

[13] J. Frijns *et al.*, "Stimulation of the facial nerve by intracochlear electrodes in otosclerosis: a computer modeling study," *Otol. Neurotol.*, vol. 30, no. 8, pp. 1168–1174, 2009.

[14] R. Saba, "Cochlear implant modelling: stimulation and power consumption," Ph.D. dissertation, Fac. of Eng. & Environ., Univ. of Southampton, Southampton, UK, 2012.

[15] P. Wong *et al.*, "Effect of petrous bone resistivities on volume conduction in the cochlea," presented at the 3rd Int. Conf. Medical Bionics, Phillip Island, Australia, Nov. 17–20, 2013.

[16] P. Tran *et al.*, "Development of HEATHER for cochlear implant stimulation using a new modeling workflow," *IEEE Trans. Biomed. Eng.*, vol. 62, no. 2, pp. 728–735, 2015.

[17] P. A. Santi, "Light Sheet Fluorescence Microscopy: A Review," *J. Histochem. Cytochem.*, vol. 59, no. 2, pp. 129-138, 2011.

[18] F. A. Spelman *et al.*, "Measurements of the resistivity of bony tissues of the cochlea," in *Proc. Ann. Int. Conf. IEEE EMBS*, 1987, pp. 1911–1912.

[19] F. A. Spelman *et al.*, "Tissue impedance and current flow in the implanted ear: implications for the cochlear prosthesis," *Ann. Otol. Rhinol. Laryngol. Suppl.*, vol. 98, no. 3, 1982.

[20] M. F. Suesserman, "Noninvasive microelectrode measurement technique for performing quantitative, in vivo measurements of inner ear tissue impedances," Ph.D. dissertation, Dept. of Elec. Eng., Univ. of Washington, Seattle, WA, 1992.

[21] C. Gabriel *et al.*, "Electrical conductivity of tissue at frequencies below 1 MHz," *Phys. Med. Biol*, vol. 54, pp. 4863–4878, 2009.

[22] S. N. Mohapatra *et al.*, "Blood resistivity and its implications for the calculation of cardiac output by the thoracic electrical impedance technique," *Intens. Care Med.*, vol 3, pp. 63–67, 1977.

[23] C. R. Johnson, "Computational methods and software for bioelectric field problems," in *Biomedical Engineering Fundamentals*, Boca Raton: CRC Press, 2006.

[24] J. J. Briaire and J. H. M. Frijns, "3D mesh generation to solve the electrical volume conduction problem in the implanted inner ear," *Simulat. Pract. Theory*, vol. 8, no. 1-2, pp. 57–73, 2000.

[25] J. A. N. Buytaert *et al.*, "MicroCT versus sTSLIM 3D imaging of the mouse cochlea," *J. Histochem. Cytochem.*, vol. 61, no. 5, pp. 382–395, 2013.

[26] P. Wong *et al.*, "Sensitivity of cochlear volume conduction models to boundary conditions," presented at the Conf. Implantable Auditory Prostheses, Lake Tahoe, CA, Jul. 14–19, 2013.
[27] C. C. Finley, "A finite-element model of radial bipolar field patterns in the electrically stimulated cochlea – two and three dimensional approximations and tissue parameter sensitivities," in *Proc. Ann. Int. Conf. IEEE EMBS*, 1989, pp. 1059–1060.
[28] R. K. Kalkman, J. J. Briaire, D. M. Dekker, and J. H. M. Frijns, "Place pitch versus electrode location in a realistic computational model of the implanted human cochlea," *Hear. Res.*, vol. 315, pp. 10–24, 2014.
[29] J. P. Reilly, *Applied bioelectricity: From electrical stimulation to electropathology*. New York: Springer-Verlag, 1998.
[30] C. Van Den Honert and D. C. Kelsall, "Focused intracochlear electric stimulation with phased array channels," *J. Acoust. Soc. Am.*, vol. 121, no. 6, pp. 3703–3716, 2007.
[31] J. Haueisen *et al.*, "Influence of tissue resistivities on neuromagnetic fields and electric potentials studied with a finite element model of the head," *IEEE Trans. Biomed. Eng.*, vol. 44, no. 8, pp. 727-735, 1997.
[32] P. A. Williams, and S. Saha, "The electrical and dielectric properties of human bone tissue and their relationship with density and bone mineral content," *Ann. Biomed. Eng.*, vol. 24, no. 2, pp. 222-233, 1996.
[33] D. Strelioff, "A computer simulation of the generation and distribution of cochlear potentials," *J. Acoust. Soc. Am.*, vol. 54, no. 3, pp. 620–629, 1973.
[34] W. M. Grill, and J. T. Mortimer, "Electrical properties of implant encapsulation tissue," *Ann. Biomed. Eng.*, vol. 22, no. 1, pp. 23–33, 1994.
[35] T. Hanekom, "Modelling encapsulation tissue around cochlear implant electrodes," *Med. Biol. Eng. Comput.*, vol. 43, no. 1, pp. 47–55, 2005.
[36] T. H. Bast and B. J. Anson, *The temporal bone and the ear*, CC Thomas, 1949.
[37] P. Dallos *et al.*, *The cochlea*, vol. 8, New York: Springer-Verlag, 1996.
[38] F. A. Spelman, "Determination of tissue impedances of the inner ear: Models and measurements," in *Cochlear Implants*, New York: Springer, 1990, pp. 35–54.
[39] G. Von Békésy, *Experiments in hearing*, vol. 8, E. G. Wever, Ed. New York: McGraw-Hill, 1960.
[40] L. E. Baker, "Principles of the impedance technique," *IEEE Eng. Med. Biol. Mag.*, vol. 8, no. 1, pp. 11–15, 1989.

Paul Wong received the B.E. (Mech. Eng. (Biomed.)) (Hons I) degree and the B.Com. degree in Finance from The University of Sydney, Camperdown, Australia, in 2010. He is currently working toward the Ph.D. degree in Biomedical Engineering at the same university in conjunction with Cochlear Ltd., Sydney, Australia.

His current research aims to improve computational models of the cochlea to better understand the spatial effects of cochlear implant stimulation.

Shefin George received the B.Tech (Biomed. Eng.) degree from Cochin University of Science and Technology, Kerala, India, in 2007, and the M.E. (Biomed.) degree from Latrobe University, Bundoora, Australia, in 2011. She is currently working towards the Ph.D. degree in Medical Bionics at the University of Melbourne in conjunction with the Bionics Institute, Melbourne, Australia.

She was a Systems Analyst at Tata Consultancy Services, India, from 2007 to 2009 and worked in smart card design and development. Following the M.E., she was a Biomedical Engineer with Chemtronics Biomedical Engineering, Australia, in 2011.

Her current research focuses on investigating current focusing stimulation techniques for cochlear implants using electrophysiological studies.

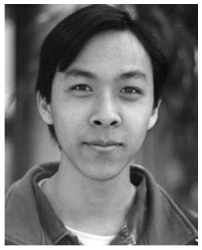

Philip Tran received the B.E. (Mech. Eng. (Biomed.)) (Hons I) degree and the B.Sc. (Adv.) degree in Chemistry from The University of Sydney, Camperdown, Australia, in 2010. He is currently working toward the Ph.D. degree in Biomedical Engineering at the same university in conjunction with Cochlear Ltd., Sydney, Australia.

His research interests include computational modeling of the human head for cochlear implant stimulation.

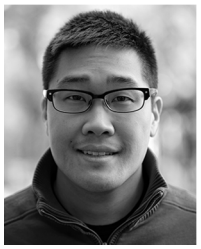

Andrian Sue received the B.E. (Mech. Eng. (Biomed.)) (Hons I) degree and the B.Med.Sc. degree from The University of Sydney, Camperdown, Australia, in 2010. He is currently working toward the Ph.D. degree in Biomedical Engineering at the same university in conjunction with Cochlear Ltd., Sydney, Australia.

His research interests include the safety of neural stimulation and the use of computational methods to predict the safety of stimulation electrodes.

Paul Carter received the B.S. degree in Physics with Solid State Electronics from the University of Exeter, U.K., in 1982, and the Ph.D. degree in microelectronics from the University of Southampton, U.K., in 1987.

He lectured in the Department of Electrical and Computing Engineering at the University of Wollongong, Australia from 1987 to 1992. He then joined Cochlear Limited, where he is currently working as Senior Principal Research Engineer, Head of Electrode Science, and Discipline Leader for Electrodes and Stimulation Safety. He also holds an Honorary Professorship in Biomedical Engineering from The University of Sydney, Australia, and is a Fellow of the Institute of Engineers, Australia.

His research interests include electroanatomical modeling, the properties of the electrode-tissue interface, and the safety of neural stimulation.

Qing Li received the Ph.D. degree in Aerospace Engineering from The University of Sydney, Camperdown, Australia, in 2000.

Following the Ph.D., he was a Postdoctoral Research Fellow at Cornell University, Ithaca, NY, USA, before returning to The University of Sydney in 2001 as an Australian Postdoctoral Fellow. He was a Senior Lecturer at James Cook University, Townsville, Australia, in 2004, and then, at The University of Sydney in 2006. He became an Associate Professor in the School of Aerospace, Mechanical and Mechatronic Engineering, The University of Sydney, in 2010. He is currently an ARC Future Fellow and Professor in Biomedical Engineering at The University of Sydney.

His current research interests include computational modeling, biomechanics, biomaterials, scaffold tissue engineering, crashworthiness, and design optimization.